Polymer 143 (2018) 324–330

Contents lists available at ScienceDirect

Polymer

journal homepage: www.elsevier.com/locate/polymer

Large negative giant magnetoresistance at room temperature and electrical transport in cobalt ferrite-polyaniline nanocomposites

Hongbo Gu [a, *], Hongyuan Zhang [a], Jing Lin [b, **], Qian Shao [c], David P. Young [e], Luyi Sun [f], T.D. Shen [g], Zhanhu Guo [d, ***]

[a] Shanghai Key Lab of Chemical Assessment and Sustainability, School of Chemical Science and Engineering, Tongji University, Shanghai, 200092, China
[b] School of Chemistry and Chemical Engineering, Guangzhou University, Guangzhou, 510006, PR China
[c] College of Chemical and Environmental Engineering, Shandong University of Science and Technology, Qingdao, 266590, China
[d] Integrated Composites Lab (ICL), Department of Chemical & Biomolecular Engineering University of Tennessee, Knoxville, TN, 37966, USA
[e] Department of Physics and Astronomy, Louisiana State University, Baton Rouge, LA, 70803, USA
[f] Department of Chemical & Biomolecular Engineering and Polymer Program, Institute of Materials Science, University of Connecticut, Storrs, CT, 06269, USA
[g] State Key Laboratory of Metastable Materials Science and Technology, Yanshan University, Hebei, 066004, China

ARTICLE INFO

Article history:
Received 19 February 2018
Received in revised form
29 March 2018
Accepted 2 April 2018
Available online 3 April 2018

Keywords:
Polyaniline nanocomposites
Cobalt ferrite
Negative magnetoresistance

ABSTRACT

At room temperature, a large negative out-of-plane magnetoresistance (MR), $[R(H)-R(0)]/R(0)$, with a value of −35.76% at magnetic field of 9 T has been obtained in the cobalt ferrite ($CoFe_2O_4$)/polyaniline (PANI) nanocomposites with $CoFe_2O_4$ loading of 40.0 wt% prepared by surface initiated polymerization (SIP) method, which is strongly related to the weak localization (WL) model in the weak disordered system. The negative MR at room temperature in the $CoFe_2O_4$/PANI nanocomposites exhibits the obvious nanoparticle loading and magnetic field dependent properties. Both thermal activated transport model and Mott variable range hopping (VRH) model are applied to express the electrical transport mechanism for the temperature regimes of 180–290 K and 50–180 K, accordingly. The electrical transport in the $CoFe_2O_4$/PANI nanocomposites obeys the 3D VRH transport mechanism at low temperature range of 50 −180 K. The estimated activation energy E_g for the $CoFe_2O_4$/PANI nanocomposites with different $CoFe_2O_4$ nanoparticle loadings of 10.0, 20.0, 40.0, and 60.0 wt% is 61, 63, 65, and 87 meV, respectively. The coating of PANI on the surface of $CoFe_2O_4$ nanoparticle reveals the significant effect on both the remanence and coercivity of $CoFe_2O_4$ nanoparticle.

1. Introduction

Recently, the great interests have been dedicated to the conducting polymer and their nanocomposites [1–3]. Polyaniline (PANI) is one of the most popular conducting polymers due to its easy synthesis, cheapness of raw material, good environmental stability and thermal stability, high electrical conductivity and reversible doping/dedoping process [4]. As one of the most important conducting polymers, PANI has the promising applications such as pesudocapacitors [5], electrochromics [6,7], bioengineering [8], bio/chemical sensors [9,10], solar cells [11], electromagnetic interference (EMI) shielding [12], and organic light emitting diodes (OLEDs) [13,14].

Owing to the particularly optical, magnetic and electrical properties, iron-based spinel metal oxide (i.e. ferrite) nanoparticles have been intensively investigated in the applications of biomedicine [15], catalyst [16], magnetic data storage [17], and energy storage [18]. Among these ferrites, the cobalt ferrite ($CoFe_2O_4$) with an inverse spinel structure, in which all Co^{2+} ions exist in octahedral sites and Fe^{3+} ions are equally dispersed between tetrahedral and octahedral sites, has been widely studied in computers, recording devices, and magnetic cards due to its high electromagnetic performance, excellent chemical stability, mechanical hardness, and high coercivity (arising from the spin coupling of cobalt and iron ions) [19]. Especially, the high magnetic anisotropy ($1.8–3 \times 10^5$ J m^{-3} at 300 K) and moderate saturation magnetization make $CoFe_2O_4$ a good candidate for magnetic resonance imaging (MRI) and high density magnetic recording media [20].

* Corresponding author.
** Corresponding author.
*** Corresponding author.
E-mail addresses: hongbogu2014@tongji.edu.cn (H. Gu), linjing@gzhu.edu.cn (J. Lin), zguo10@utk.edu (Z. Guo).

https://doi.org/10.1016/j.polymer.2018.04.008
0032-3861/

Recently, the nanocomposites composed of $CoFe_2O_4$ and PANI have been intensively investigated. Yet, most of researches focus on the $CoFe_2O_4$/PANI nanocomposites regarding their microwave absorption properties [21,22], electrical conductivity [23], humidity sensing properties [24], magnetic and electrochemical properties [25].

Giant magnetoresistance (GMR) is the resistance change of a material under an external magnetic field (H) [26]. Normally, the positive and negative GMR mean the increase and the decrease in resistance of a material under the applied magnetic field, respectively, which implies that the resistance of a material can be tuned by the external magnetic field. In recent years, GMR phenomenon has been reported in the PANI and its nanocomposites. For example, Gu et al. have found a large GMR value of 95% in the magnetic Fe_3O_4/PANI nanocomposites with a Fe_3O_4 nanoparticle loading of 30 wt% [27] and a large GMR value of 95.5% in the non-magnetic silica/PANI nanocomposites with a silica nanoparticle loading of 20 wt% at room temperature [28]. Zhu et al. have reported a GMR value up to 30% in the 5 wt% loading of graphene/PANI nanocomposites at room temperature [29]. However, these studies mostly concentrated on the positive GMR values, the work related to the negative GMR in the PANI nanocomposites at room temperature is rarely reported.

In this work, a large negative GMR in the $CoFe_2O_4$/PANI nanocomposites filled with different $CoFe_2O_4$ nanoparticle loadings at room temperature has been reported. The chemical structures of $CoFe_2O_4$/PANI nanocomposites are characterized by Fourier transform infrared (FT-IR) spectroscopy. The thermal stability of $CoFe_2O_4$/PANI nanocomposites is conducted by thermogravimetric analysis (TGA). The scanning electron microscope (SEM) and transmission electron microscopy (TEM) are applied to observe the microstructures of $CoFe_2O_4$/PANI nanocomposites. The electrical transport mechanism is systematically investigated by the temperature dependent resistivity measurements through the thermal activated transport model and Mott variable range hopping (VRH) model. The MR properties in $CoFe_2O_4$/PANI nanocomposites are explained by the weak localization in the weak disordered system. The effect of PANI on the magnetic properties including remanence and coercivity of $CoFe_2O_4$ is also studied.

2. Experimental

2.1. Materials

Ammonium persulfate (APS, $(NH_4)_2S_2O_8$), aniline (C_6H_7N) and *p*-toluene sulfonic acid (PTSA, $C_7H_8O_3S$) were provided by Sigma Aldrich. The cobalt ferrite ($CoFe_2O_4$) nanoparticles with an average diameter of 35–55 nm (98%) were obtained from Nanostructured & Amorphous Materials, Inc. All the chemicals were used as-received without any further treatment.

2.2. Fabrication of cobalt ferrite/polyaniline nanocomposites

A surface initiated polymerization (SIP) method was used to synthesize the $CoFe_2O_4$/PANI nanocomposites. Firstly, $CoFe_2O_4$ nanoparticles (0.37–3.02 g), APS (18 mmol) and PTSA (30 mmol) were added into 200 mL of deionized water in an ice-water bath for 1-h mechanical stirring (SCILOGEX OS20-Pro LCD Digital Overhead Stirrer, 300 rpm) combined with sonication (Branson 8510). Then the aniline solution (36 mmol) was dripped into above solution and continuously stirred for further polymerization in an ice-water bath. After that, the product was vacuum filtered and washed with deionized water and ethanol to remove any residual oxidant and possible oligomers. The final powders were dried at 60 °C in a regular oven overnight. The $CoFe_2O_4$/PANI nanocomposites with a $CoFe_2O_4$ nanoparticle loading of 10.0, 20.0, 40.0 and 60.0 wt% were prepared. In comparison, pure PANI was also synthesized following the same procedures without adding any $CoFe_2O_4$ nanoparticles.

2.3. Characterizations

A Bruker Inc. Vector 22 (coupled with an ATR accessory) was used to capture the FT-IR spectra of these products in the range of 500–2500 cm^{-1} at a resolution of 4 cm^{-1}. The microstructures of the synthesized nanocomposites were observed on a field emission scanning electron microscope (SEM, JEOL, JSM-6700F system) and a transmission electron microscopy (TEM, FEI Tecnai G2 F20). A TGA Q-500 equipment from TA instruments was applied to conduct TGA with a heating rate of 10 °C min^{-1} under an air flow rate of 60 mL min^{-1} from 30 to 800 °C.

The pure PANI and its $CoFe_2O_4$ nanocomposites were pressed in a form of disc pellet with a diameter of 25 mm by applying a pressure of 50 MPa in a hydraulic presser and an average thickness of 1.0 mm for measuring the temperature dependent resistivity (ρ) by a standard four-probe method from 50 to 290 K. The magnetic property was carried out in a 9-T Physical Properties Measurement System (PPMS) by Quantum Design at room temperature. The magnetoresistance (MR) was investigated by a standard four-probe technique with the magnetic field applied perpendicular to the current.

3. Results and discussion

3.1. Characterization of cobalt ferrite/polyaniline nanocomposites

In the FT-IR spectrum of pure PANI, Fig. 1(A)–a, the absorption peaks around 1479 and 1559 cm^{-1} are attributed to the C=C stretching vibration of the benzenoid and quinoid rings, respectively [30]. The band at 1292 cm^{-1} is assigned to the C-N stretching vibration of secondary amine, which is a characteristic band for the conducting emeraldine salt (ES) form of PANI generating from its bipolaron structure [31]. The peaks at 1235 and 785 cm^{-1} correspond to the C-N stretching vibration of the polaronic structures and the out-of-plane bending of C-H in the substituted benzenoid ring, respectively [32]. These peaks are the characteristic FT-IR spectrum of PANI [33]. However, they have shifted to the higher wavenumbers in the $CoFe_2O_4$/PANI nanocomposites, Fig. 1(A)-b&c&d&e, indicating a strong interaction between $CoFe_2O_4$ nanoparticles and PANI associated with the charge delocalization on the polymer backbone of PANI [34]. This indicates the successful synthesis of $CoFe_2O_4$/PANI nanocomposites. Meanwhile, in the $CoFe_2O_4$/PANI nanocomposites, the absorption peak at around ~550 cm^{-1} is the stretching vibration of M – O clusters originated from $CoFe_2O_4$ in the tetrahedral sites [35].

The thermal stability of pure PANI and $CoFe_2O_4$/PANI nanocomposites with different $CoFe_2O_4$ nanoparticle loadings is investigated and the obtained TGA curves in the air condition are displayed in Fig. 1(B). The pure PANI and $CoFe_2O_4$/PANI nanocomposites exhibit the similar decomposition profiles with two-stage degradations [36,37]. The first stage within the temperature range from room temperature to 200 °C arises from the evaporation of moisture and the doped acid PTSA in PANI polymer structure. The second stage, as the major weight loss, from 300 to 600 °C is due to the complex thermal degradation of PANI polymer chains [38]. It's observed that the presence of $CoFe_2O_4$ could significantly improve the thermal stability of PANI. The thermal stability of $CoFe_2O_4$/PANI nanocomposites is increased with increasing $CoFe_2O_4$ nanoparticle loadings. The 15% weight loss decomposition temperature for pure PANI and $CoFe_2O_4$/PANI nanocomposites with a $CoFe_2O_4$ nanoparticle loading of 10.0, 20.0, 40.0 and 60.0 wt% is

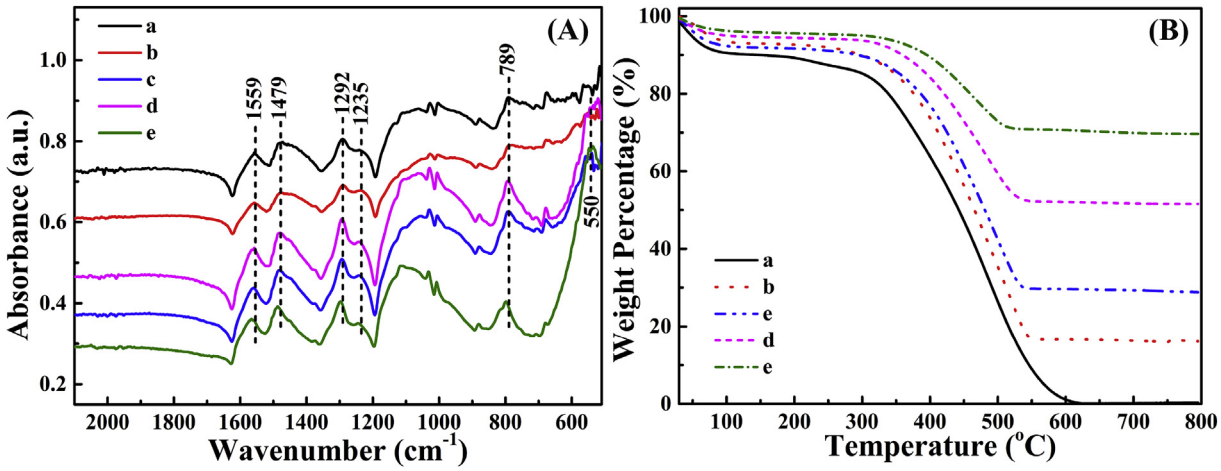

Fig. 1. (A) FT-IR spectra and (B) TGA curves of (a) pure PANI; the $CoFe_2O_4$/PANI nanocomposites with a nanoparticle loading of (b) 10.0, (c) 20.0, (d) 40.0 and (e) 60.0 wt%.

303, 349, 356, 395 and 431 °C, accordingly. The pure PANI is almost completely decomposed at 800 °C, whereas the weight residues of the nanocomposites with an initial $CoFe_2O_4$ nanoparticle loading of 10.0, 20.0, 40.0 and 60.0 wt% at 800 °C are 16.12, 28.82, 51.58 and 69.66%, respectively. The weight residues in the nanocomposites are different from the initially calculated $CoFe_2O_4$ nanoparticle loading based on the aniline monomers and $CoFe_2O_4$ nanoparticles during the experiment, which may involve in the incomplete polymerization of the aniline monomers [39].

Fig. 2&S1 shows the SEM microstructures of as-received $CoFe_2O_4$ nanoparticles, $CoFe_2O_4$/PANI nanocomposites with $CoFe_2O_4$ nanoparticle loading of 10.0 and 60.0 wt% and pure PANI, respectively. The pure PANI nanoparticles seems like sticky together, Figure S1. The $CoFe_2O_4$ nanoparticles are observed to have a fairly smooth and particulate surface, Fig. 2(a), whereas 10.0 wt% loading of $CoFe_2O_4$/PANI nanocomposites exhibit a rough and flake-like surface, Fig. 2(b). Even 60.0 wt% loading of $CoFe_2O_4$/PANI nanocomposites still possess a particulate structure, the presence of PANI on the surface of $CoFe_2O_4$ nanoparticle makes it rough, Fig. 2(c), implying the polymerization of aniline taken place on the surface of $CoFe_2O_4$ nanoparticle [40,41]. This is also found in the TEM images of as-received $CoFe_2O_4$ nanoparticles and $CoFe_2O_4$/PANI nanocomposites, Figure S2. In Figure S2(a), for the as-received $CoFe_2O_4$ nanoparticles, the diameters of nanoparticles are around 35–55 nm, which is consistent with the results provided by Nanostructured & Amorphous Materials, Inc. In Figure S2(b), for the $CoFe_2O_4$/PANI nanocomposites with a $CoFe_2O_4$ nanoparticle loading of 60.0 wt%, the obvious amorphous polymer layers are present outside of $CoFe_2O_4$ nanoparticles, indicating the polymerization of aniline on the surface of $CoFe_2O_4$ nanoparticles [42–44]. All of these results including FT-IR, TGA, SEM, and TEM confirm the successful fabrication of $CoFe_2O_4$/PANI nanocomposites.

3.2. Temperature dependent electrical transport in cobalt ferrite/polyaniline nanocomposites

In this work, the electrical transport of $CoFe_2O_4$/PANI nanocomposites with different $CoFe_2O_4$ nanoparticle loadings is investigated within a wide temperature range from 50 to 290 K. The temperature dependent resistivity curves are depicted in Fig. 3(A). The non-linear resistivity change with temperature are noticed for all the prepared $CoFe_2O_4$/PANI nanocomposites, in which the resistivity decreases with increasing temperature and exhibits a typical semiconducting behavior in the measured temperature range from 50 to 290 K [45]. Meanwhile, at lower temperature (below 180 K), the resistivity is grown rapidly with decreasing temperature, whereas at higher temperature the resistivity slightly changes after further increasing temperature. It's also seen that the resistivity rises with increasing $CoFe_2O_4$ nanoparticle loadings since the existence of $CoFe_2O_4$ nanoparticles may affect the interaction between PANI polymer matrix and doped acid, partially blocking the charge carriers transport pathway [46,47]. The resistivity for the $CoFe_2O_4$/PANI nanocomposites with $CoFe_2O_4$ nanoparticle loading of 10.0, 20.0, and 40.0 wt% is changed from $10^2\,\Omega$ cm at 290 K to $10^5\,\Omega$ cm at 50 K. However, for the $CoFe_2O_4$/PANI nanocomposites with a $CoFe_2O_4$ nanoparticle loading of 60.0 wt%, the resistivity is $10^4\,\Omega$ cm at 290 K and increases to $10^5\,\Omega$ cm at 110 K. Since this resistivity value of $10^5\,\Omega$ cm for 60.0 wt % of $CoFe_2O_4$/PANI nanocomposites almost reaches the maximum value of the measured equipment, the resistivity for this sample can't be obtained as the temperature is lower than 110 K.

Normally, the possible electrical conduction mechanism in the disordered semiconducting materials can be explained by the thermally activated transport and Mott VRH mechanism [48]. Therefore, in this work, this non-linear behavior of resistivity with temperature in the $CoFe_2O_4$/PANI nanocomposites is explored in the two different temperature regimes with these two mechanisms to investigate their electrical transport behaviors. The first regime is at higher temperature range from 180 to 290 K and the results are analyzed based on the thermal activated transport [49,50] equation as shown in eq (1):

$$R(T) = R_0 \exp\left(\frac{E_g}{k_B T}\right) \quad (1)$$

where R_0 is a constant, E_g stands for the activation energy, and k_B is Boltzmann constant. With the linear fit of $\ln(R) \sim T^{-1}$ (the data from 180 to 290 K are captured from Fig. 3(A)), E_g and R_0 can be respectively obtained from the slope and the intercept of plot. The corresponding fitting results for the $CoFe_2O_4$/PANI nanocomposites with different $CoFe_2O_4$ nanoparticle loadings are shown in Fig. 3(B) and the estimated E_g and R_0 are listed in Table 1. The calculated activation energy E_g for the $CoFe_2O_4$/PANI nanocomposites with different $CoFe_2O_4$ nanoparticle loading of 10.0, 20.0, 40.0, and 60.0 wt% is correspondingly 61, 63, 65, and 87 meV and increases with increasing $CoFe_2O_4$ nanoparticle loadings as expected. Especially, the E_g for the 60.0 wt% loading of $CoFe_2O_4$/PANI nanocomposites is much higher than $CoFe_2O_4$/PANI nanocomposites with nanoparticle loadings of 10.0, 20.0, and 40.0 wt%, which is

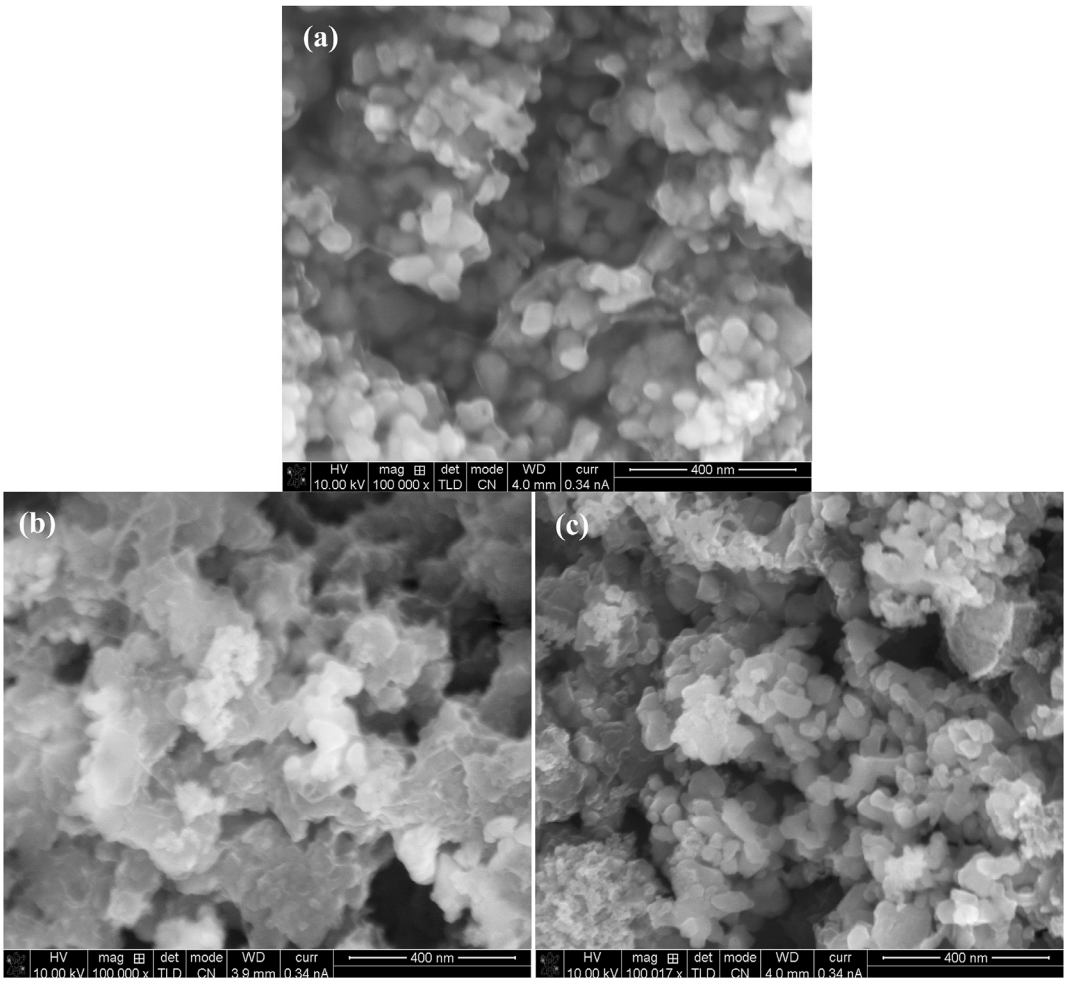

Fig. 2. SEM microstructures of (a) as-received $CoFe_2O_4$ nanoparticles; $CoFe_2O_4$/PANI nanocomposites with $CoFe_2O_4$ loading of (b) 10.0 and (c) 60.0 wt%.

consistent with the obtained resistivity results for $CoFe_2O_4$/PANI nanocomposites in the temperature range of 180–290 K as mentioned above.

VRH conduction mechanism is proposed by Mott to describe the charge transport in the disordered system at low temperature, in which the conduction is induced by the phonon-assisted tunneling between the localized states centered at different positions [51,52]. The general expression for Mott VRH mechanism is denoted as eq (2):

$$\sigma = \sigma 0 \exp\left[-\left(\frac{T0}{T}\right)^{1/n+1}\right], \cdot n = 1, 2, \cdot 3 \quad (2)$$

where σ_0 is also a constant, T_0 represents the Mott characteristic temperature. The value $n = 1$ is related to the Efros-Shklovskii variable range hopping (ES-VRH), and $n = 2$ and 3 in corresponds to 3- and 2-D VRH models, respectively. In this work, the second regime at lower temperature from 50 to 180 K is examined by Mott VRH mechanism. The relevant plot of $\ln(\sigma) \sim T^{-1/(n+1)}$(the data are acquired from Fig. 3(A)) is drawn in Fig. 3(C). The σ_0 and T_0 can be gained by the intercept and the slope of this plot. After fitting, it's found that the temperature dependent resistivity within the temperature range of 50–180 K for $CoFe_2O_4$/PANI nanocomposites obeys a $\ln(\sigma) \sim T^{-1/4}$ linear relationship when $n = 3$, implying a quasi 3D VRH electrical conduction mechanism. The σ_0 and T_0 are computed and also summarized in Table 1. Both σ_0 and T_0 in the $CoFe_2O_4$/PANI nanocomposites increase with increasing $CoFe_2O_4$ nanoparticle loadings. The higher T_0 usually means the stronger charge carrier scattering and the higher energy needed for charge carrier's hopping [53].

3.3. Magnetoresistance (MR)

Generally, the measured GMR signal is not related to the strength of applied magnetic field, but also correlated with the direction of the magnetic field relative to the current as well as the measured temperature [54]. Therefore, it's often needed to point out the strength of magnetic field, the direction of the magnetic field to the current, and the temperature for measured GMR value. The out-of-plane MR measurements (i.e. the magnetic field is perpendicular to the current) were conducted at 290 K and the calculated MR% = [$R(H)$ - $R(0)$]/$R(0)$ × 100% are displayed in Fig. 4(A). It's found that the MR for all the $CoFe_2O_4$/PANI nanocomposites is negative within the measured magnetic field range and the absolute value of MR increases with increasing $CoFe_2O_4$ nanoparticle loading to 40 wt% (The MR% value at 9 T is respectively −7.01, −19.61, and −35.76% for $CoFe_2O_4$/PANI nanocomposites with nanoparticle loading of 10.0, 20.0, and 40.0 wt%.) and then decreases as $CoFe_2O_4$ nanoparticle loading increases to 60.0 wt% (the MR value is −26.44%).

It's reported that the forward interference model can be applied to explain the negative MR value in the materials, in which the

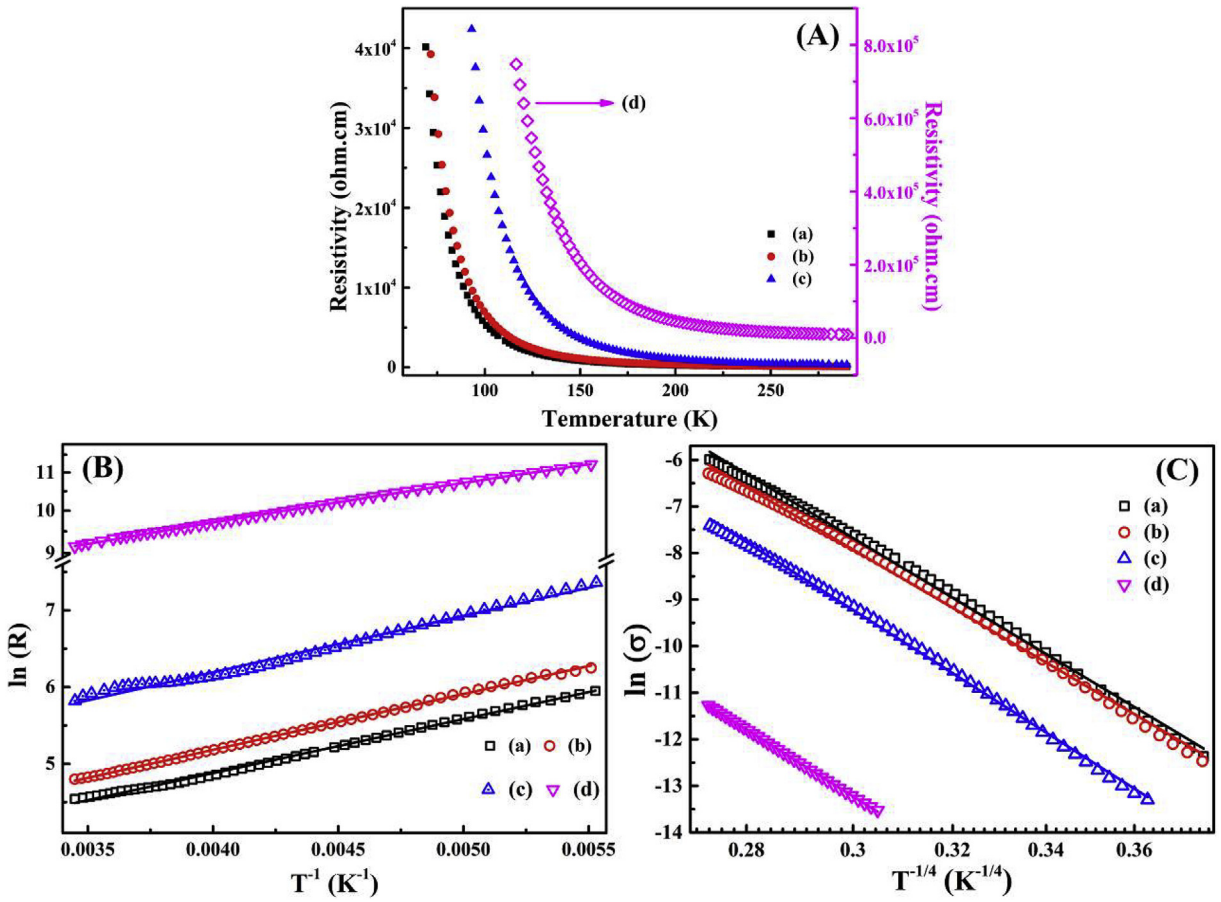

Fig. 3. (A) Resistivity *vs.* temperature, (B) ln (R) ~ T^{-1} plotted within temperature range of 180 ~ 290 K, and (C) ln (σ) ~ $T^{-1/4}$ curves of $CoFe_2O_4$/PANI nanocomposites with different $CoFe_2O_4$ nanoparticle loadings.

Table 1
R_0, E_g, σ_0, and T_0 for the different loadings of $CoFe_2O_4$/PANI nanocomposites.

Samples	R_0	E_g (meV)	r^2 (1st)	σ_0 (S cm^{-1})	$T_0 \times 10^7$ (K)	r^2 (2nd)
10.0 wt% $CoFe_2O_4$	7.87	61	0.997	4488	1.39	0.997
20.0 wt% $CoFe_2O_4$	9.67	63	0.999	34984	1.54	0.997
40.0 wt% $CoFe_2O_4$	26.08	65	0.988	62670	2.06	0.998
60.0 wt% $CoFe_2O_4$	293.02	87	0.999	70558	5.53	0.999

effect of interference among various hopping paths is believed to be the main reason for the negative MR effect [55]. The symbolic representation for the forward interference model is described as eq (3):

$$R(H,T)/R(0,T) \approx 1/\{1 + C_{sat}[H/H_{sat}]/[1 + H/H_{sat}]\} \quad (3)$$

where $R(H, T)/R(0, T)$ stands for the resistance ratio, the fitting parameters C_{sat} and H_{sat} are constants. H_{sat} is given by eq (4):

$$H_{sat} \approx 0.7\left(\frac{8}{3}\right)^{3/2}\left(\frac{1}{a_0^2}\right)\left(\frac{h}{e}\right)\left(\frac{T}{T_0}\right)^{3/8} \quad (4)$$

where h is Planck's constant, e is electron charge and T_0 is the Mott characteristic temperature (K). The corresponding ratio $R(H)/R(0)$ as a function of H is shown in Fig. 4(B). After fitting $R(H)/R(0) \sim H$ by Polymath software, the obtained C_{sat} value for $CoFe_2O_4$/PANI nanocomposites with nanoparticle loading of 10.0, 20.0, 40.0, and 60.0 wt% is 0.042, 0.130, 0.332, and 0.172, respectively. The estimated a_0 for $CoFe_2O_4$/PANI nanocomposites with different nanoparticle loadings at different H regarding eq (4) is listed in Table S1. It's observed that the a_0 for $CoFe_2O_4$/PANI nanocomposites is dependent on the applied magnetic field and decreases as magnetic field increases. In addition, the calculated a_0 is very large with a value of about 251.3 nm for $CoFe_2O_4$/PANI nanocomposites with 10 wt% loading of $CoFe_2O_4$ nanoparticles at a magnetic field of 0.10 T, which suggests that the localization in these samples is very weak. Normally, the wave propagation within random potentials can be used to understand the electrical transport properties in the disordered systems, which is called “localization”, a consequence of coherent back scattering of electron waves scattered by the impurities [56]. For the strong localization (strong disorder system), the electrical transport arises from the hopping, leading to an increased localization length and positive magnetoresistance [57]. However, in the weak localization (weak disordered system), the perpendicular magnetic field breaks the time reversal symmetry and induces a phase shift in wave function, which inhibit the backscattering. Meanwhile, a constructive interference resulted

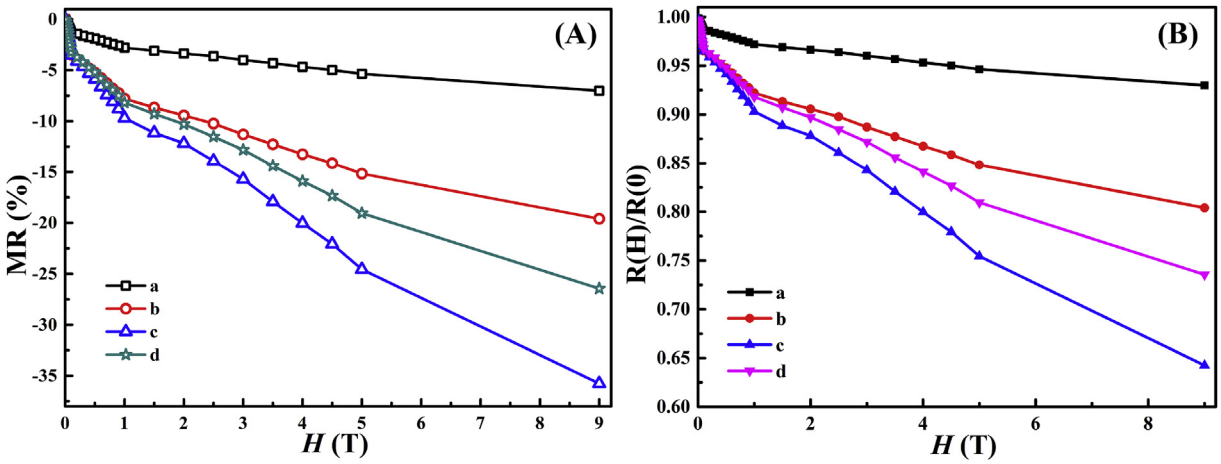

Fig. 4. (A) Magnetoresistance and (B) ratio of R(H)/R(0) as a function of H for $CoFe_2O_4$/PANI nanocomposites with $CoFe_2O_4$ nanoparticle loading of (a) 10.0, (b) 20.0, (c) 40.0, and (d) 60.0 wt% at T = 290 K.

from the coherence in single electron scattering paths is also established and in turn devotes to the resistance [58]. Both of these two reasons cause the negative magnetoresistance value in the $CoFe_2O_4$/PANI nanocomposites.

3.4. Magnetic property

The magnetic hysteresis loops of as-received $CoFe_2O_4$ nanoparticles, and $CoFe_2O_4$/PANI nanocomposites with different $CoFe_2O_4$ nanoparticle loadings at room temperature are demonstrated in Fig. 5. It's noticed that the magnetization of these samples isn't saturated at the magnetic field of 20000 Oe, thereby, the saturation magnetization (M_s, at which the magnetic moments are aligned to the direction of magnetic field and saturate the magnetization [59,60]) is determined by the extrapolated magnetization calculated from the intercept of $M \sim H^{-1}$ at high magnetic field [61]. The M_s of as-received $CoFe_2O_4$ nanoparticles is 61.43 emu g^{-1}, which is appropriate 82.92% of bulk value for barium ferrite (74.08 emu g^{-1}) [19]. This relatively reduced M_s value for the $CoFe_2O_4$ nanoparticles compared to the bulk materials may be originated from the structural distortion on the surface of nanoparticles, which decreases the contribution of magnetic moments [62]. It's also reported that the magnetic behavior in ferromagnetic materials possesses the particle size dependence, which is one of the reasons for this changed M_s in the $CoFe_2O_4$ nanoparticles (the nanosized particles possess quantum size effect) [15]. In addition, the M_s of $CoFe_2O_4$/PANI nanocomposites with $CoFe_2O_4$ nanoparticle loadings of 10.0, 20.0, 40.0, and 60.0 wt% is simultaneously estimated by the same method and the corresponding M_s value is 8.34, 17.45, 32.81, and 44.02 emu g^{-1}, separately. The difference in the M_s for $CoFe_2O_4$/PANI nanocomposites from that of the $CoFe_2O_4$ nanoparticles is because of the different loadings of $CoFe_2O_4$ nanoparticles in the nanocomposites, from which the weight percentage of $CoFe_2O_4$ nanoparticles in the nanocomposites can be estimated to be around 13.6, 28.41, 53.41, and 71.66%. These results are consistent with the weight residue obtained from TGA curve as aforementioned. There is certainly obvious hysteresis loop in the magnetization curves of as-received $CoFe_2O_4$ nanoparticles, and $CoFe_2O_4$/PANI nanocomposites since $CoFe_2O_4$ is one of the hard magnetic materials [63]. Normally, there are two characteristic parameters in the hysteresis loops for the ferromagnetic materials, i.e. remanence and coercivity. The remanence (M_r, also called remnant magnetization, which is the residual magnetization after the magnetic field is removed) for the $CoFe_2O_4$ nanoparticles and

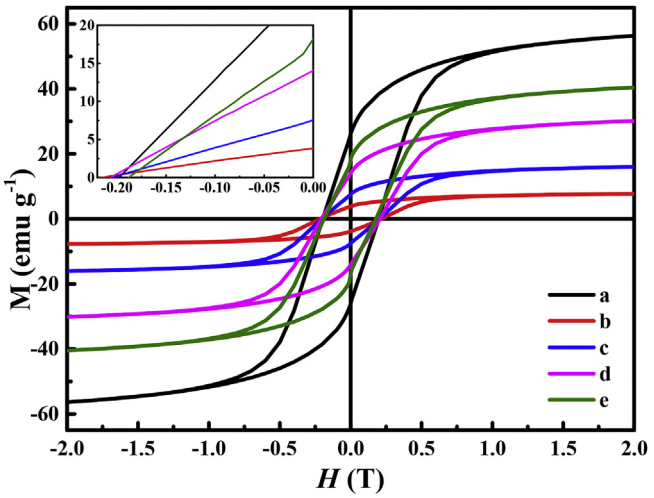

Fig. 5. Hysteresis loops of (a) as-received $CoFe_2O_4$ nanoparticles; $CoFe_2O_4$/PANI nanocomposites with $CoFe_2O_4$ loading of (b) 10.0, (c) 20.0, (d) 40.0, and (e) 60.0 wt% at room temperature.

$CoFe_2O_4$/PANI nanocomposites with nanoparticle loading of 10.0, 20.0, 40.0, and 60.0 wt%, read from the *y* axis is around 26.13, 3.84, 7.55, 14.05, and 18.17 emu g^{-1}, respectively. The coercivity (H_c) of the $CoFe_2O_4$ nanoparticles and $CoFe_2O_4$/PANI nanocomposites with nanoparticle loading of 10.0, 20.0, 40.0, and 60.0 wt%, obtained from the *x* axis crossover as shown in the inset of Fig. 5, is 1.97, 2.19, 2.03, 2.07, and 1.87 kOe, accordingly. The highly coercive $CoFe_2O_4$ nanoparticles and $CoFe_2O_4$/PANI nanocomposites are hard materials and represent the permanent magnets [64]. Compared with the $CoFe_2O_4$ nanoparticles, the difference of H_c in the $CoFe_2O_4$/PANI nanocomposites may be derived from the defects manufactured in the polymerization process of aniline, which might act as the pinning centers during the magnetization reversal [65].

4. Conclusions

The $CoFe_2O_4$/PANI nanocomposites with different $CoFe_2O_4$ nanoparticle loadings have been prepared by a SIP method. The FT-IR, TGA, SEM and TEM results confirm the successful synthesis of PANI coated $CoFe_2O_4$ nanocomposites. The presence of $CoFe_2O_4$ nanoparticles could enhance the thermal stability of PANI and the

thermal stability of $CoFe_2O_4$/PANI nanocomposites is improved as $CoFe_2O_4$ nanoparticle loading increases. The resistivity of $CoFe_2O_4$/PANI nanocomposites is increased with decreasing temperature and increasing $CoFe_2O_4$ nanoparticle loadings. The electrical transport in the $CoFe_2O_4$/PANI nanocomposites within the temperature regime of 180–290 K follows the thermal activated transport mechanism and obeys a quasi 3D VRH electrical conduction mechanism for the temperature range from 50 to 180 K. A large negative out-of-plane GMR with a value of −35.76% is obtained in the $CoFe_2O_4$/PANI nanocomposites with 40.0 wt% loading of $CoFe_2O_4$ nanoparticle. The negative MR is well explained by the weak localization model in the weak disordered system as confirmed by forward interference model. The fabrication of PANI on the surface of $CoFe_2O_4$ nanoparticles has obvious effects on both the remanence and the coercivity arising from the defects created during the polymerization of aniline.

Acknowledgement

The authors are grateful for the support and funding from the Foundation of National Natural Science Foundation of China (Nos. 51703165), and Young Elite Scientist Sponsorship Program by CAST (YESS, No. 2016QNRC001). This work is supported by Shanghai Science and Technology Commission (14DZ2261100).

Appendix A. Supplementary data

Supplementary data related to this article can be found at https://doi.org/10.1016/j.polymer.2018.04.008.

References

[1] X. Lu, W. Zhang, C. Wang, T.-C. Wen, Y. Wei, Prog. Polym. Sci. 36 (5) (2011) 671–712.
[2] H. Gu, C. Liu, J. Zhu, J. Gu, E.K. Wujcik, L. Shao, N. Wang, H. Wei, R. Scaffaro, J. Zhang, Z. Guo, Adv Compos Hybrid Mater 1 (1) (2018) 1–5.
[3] X. Xu, H. Zhang, H. Lou, C. Ma, Y. Li, Z. Guo, H. Gu, Eng. Sci. (2018), https://doi.org/10.30919/espub.es.180308.
[4] C. Oueiny, S. Berlioz, F.-X. Perrin, Prog. Polym. Sci. 39 (4) (2014) 707–748.
[5] (a) T. Liu, L. Finn, M. Yu, H. Wang, T. Zhai, X. Lu, Y. Tong, Y. Li, Nano Lett. 14 (5) (2014) 2522–2527;
(b) X. Wang, X. Zeng, D. Cao, Eng. Sci. (2018), https://doi.org/10.30919/es.180325.
[6] H. Wei, X. Yan, S. Wu, Z. Luo, S. Wei, Z. Guo, J. Phys. Chem. C 116 (47) (2012) 25052–25064.
[7] H. Wei, H. Gu, J. Guo, D. Cui, X. Yan, J. Liu, D. Cao, X. Wang, S. Wei, Z. Guo, Adv Compos Hybrid Mater 1 (1) (2018) 127–134.
[8] T.H. Qazi, R. Rai, A.R. Boccaccini, Biomaterials 35 (33) (2014) 9068–9086.
[9] I. Fratoddi, I. Venditti, C. Cametti, M.V. Russo, Sens. Actuators, B 220 (Supplement C) (2015) 534–548.
[10] Z. Sun, L. Zhang, F. Dang, Y. Liu, Z. Fei, Q. Shao, H. Lin, J. Guo, L. Xiang, N. Yerra, Z. Guo, CrystEngComm 19 (24) (2017) 3288–3298.
[11] A. Moayeri, A. Ajji, Synth. Met. 200 (2015) 7–15.
[12] P. Saini, M. Arora, G. Gupta, B.K. Gupta, V.N. Singh, V. Choudhary, Nanoscale 5 (10) (2013) 4330–4336.
[13] M.-R. Choi, T.-H. Han, K.-G. Lim, S.-H. Woo, D.H. Huh, T.-W. Lee, Angew. Chem. Int. Ed. 123 (28) (2011) 6398–6401.
[14] M. Jaymand, Prog. Polym. Sci 38 (9) (2013) 1287–1306.
[15] M.M. El-Okr, M.A. Salem, M.S. Salim, R.M. El-Okr, M. Ashoush, H.M. Talaat, J. Magn. Magn Mater. 323 (7) (2011) 920–926.
[16] A. Al-Anazi, W.H. Abdelraheem, C. Han, M.N. Nadagouda, L. Sygellou, M.K. Arfanis, P. Falaras, V.K. Sharma, D.D. Dionysiou, Appl. Catal., B 221 (2018) 266–279.
[17] L.T. Lu, N.T. Dung, L.D. Tung, C.T. Thanh, O.K. Quy, N.V. Chuc, S. Maenosono, N.T.K. Thanh, Nanoscale 7 (46) (2015) 19596–19610.
[18] Q.Q. Xiong, J.P. Tu, S.J. Shi, X.Y. Liu, X.L. Wang, C.D. Gu, J. Power Sources 256 (2014) 153–159.
[19] M.G. Naseri, E.B. Saion, H.A. Ahangar, A.H. Shaari, M. Hashim, J. Nanomater. 2010 (2010) 1–8.
[20] G. Wang, Y. Ma, Z. Wei, M. Qi, Chem. Eng. J. 289 (2016) 150–160.
[21] N. Gandhi, K. Singh, A. Ohlan, D.P. Singh, S.K. Dhawan, Compos. Sci. Technol. 71 (15) (2011) 1754–1760.
[22] C. Yang, J. Jiang, X. Liu, C. Yin, C. Deng, J. Magn. Magn Mater. 404 (2016) 45–52.
[23] E.E. Tanrıverdi, A.T. Uzumcu, H. Kavas, A. Demir, A. Baykal, Nano-micro Lett. 3 (2) (2011) 99–107.
[24] N. Parvatikar, S. Jain, C.M. Kanamadi, B.K. Chougule, S.V. Bhoraskar, M.V.N.A. Prasad, J. Appl. Polym. Sci. 103 (2) (2007) 653–658.
[25] N. Dong, M. Zhong, P. Fei, Z. Lei, B. Su, J. Alloy. Comp 660 (2016) 382–386.
[26] C.L. Chien, J.Q. Xiao, J.S. Jiang, J. Appl. Phys 73 (10) (1993) 5309–5314.
[27] H. Gu, Y. Huang, X. Zhang, Q. Wang, J. Zhu, L. Shao, N. Haldolaarachchige, D.P. Young, S. Wei, Z. Guo, Polymer 53 (3) (2012) 801–809.
[28] H. Gu, J. Guo, X. Zhang, Q. He, Y. Huang, H.A. Colorado, N. Haldolaarachchige, H. Xin, D.P. Young, S. Wei, Z. Guo, J. Phys. Chem. C 117 (12) (2013) 6426–6436.
[29] J. Zhu, H. Gu, Z. Luo, N. Haldolaarachige, D.P. Young, S. Wei, Z. Guo, Langmuir 28 (27) (2012) 10246–10255.
[30] H. Gu, H. Zhang, C. Ma, S. Lyu, F. Yao, C. Liang, X. Yang, J. Guo, Z. Guo, J. Gu, J. Phys. Chem. C 121 (24) (2017) 13265–13273.
[31] K. Singh, A. Ohlan, V.H.,R.B. Pham, S. Varshney, J. Jang, S.H. Hur, W.M. Choi, M. Kumar, S.K. Dhawan, B.-S. Kong, J.S. Chung, Nanoscale 5 (6) (2013) 2411–2420.
[32] H.-P. Cong, X.-C. Ren, P. Wang, S.-H. Yu, Energy Environ. Sci. 6 (4) (2013) 1185–1191.
[33] S.K. Pillalamarri, F.D. Blum, A.T. Tokuhiro, J.G. Story, M.F. Bertino, Chem. Mater. 17 (2) (2004) 227–229.
[34] J. Zhu, S. Wei, L. Zhang, Y. Mao, J. Ryu, A.B. Karki, D.P. Young, Z. Guo, J. Mater. Chem. 21 (2011) 342–348.
[35] (a) B. Xiang, D. Ling, H. Lou, H. Gu, J. Hazard. Mater. 325 (2017) 178–188;
(b) H. Gu, X. Xu, H. Zhang, C. Liang, H. Lou, C. Ma, Y. Li, Z. Guo, J. Gu, Eng. Sci. (2018), https://doi.org/10.30919/espub.es.180308.
[36] H. Gu, C. Ma, C. Liang, X. Meng, J. Gu, Z. Guo, J. Mater. Chem. C 5 (17) (2017) 4275–4285.
[37] Y. Guo, G. Xu, X. Yang, K. Ruan, T. Ma, Q. Zhang, J. Gu, Y. Wu, H. Liu, Z. Guo, J. Mater. Chem. C 6 (12) (2018) 3004–3015.
[38] J.R. Potts, D.R. Dreyer, C.W. Bielawski, R.S. Ruoff, Polymer 52 (1) (2011) 5–25.
[39] C. Liang, P. Song, H. Gu, C. Ma, Y. Guo, H. Zhang, X. Xu, Q. Zhang, J. Gu, Composites Part A 102 (2017) 126–136.
[40] H. Gu, J. Guo, Q. He, Y. Jiang, Y. Huang, N. Haldolaarachige, Z. Luo, D.P. Young, S. Wei, Z. Guo, Nanoscale 6 (1) (2014) 181–189.
[41] Y. Ma, L. Lv, Y. Guo, Y. Fu, Q. Shao, T. Wu, S. Guo, K. Sun, X. Guo, E.K. Wujcik, Z. Guo, Polymer 128 (2017) 12–23.
[42] S. Mondal, S. Ganguly, P. Das, D. Khastgir, N.C. Das, Composites Part B 119 (2017) 41–56.
[43] S. Mondal, P. Das, S. Ganguly, R. Ravindren, S. Remanan, P. Bhawal, T.K. Das, N.C. Das, Composites Part A 107 (2018) 447–460.
[44] C. Wang, M. Zhao, J. Li, J. Yu, S. Sun, S. Ge, X. Guo, F. Xie, B. Jiang, E.K. Wujcik, Y. Huang, N. Wang, Z. Guo, Polymer 131 (2017) 263–271.
[45] H. Liu, A.T. Neal, Z. Zhu, Z. Luo, X. Xu, D. Tománek, P.D. Ye, ACS Nano 8 (4) (2014) 4033–4041.
[46] S. Mondal, L. Nayak, M. Rahaman, A. Aldalbahi, T.K. Chaki, D. Khastgir, N.C. Das, Composites Part B 109 (2017) 155–169.
[47] S. Mondal, S. Ganguly, P. Das, P. Bhawal, T.K. Das, R. Ravindren, S. Ghosh, N.C. Das, Mater. Sci. Eng. B 225 (2017) 140–149.
[48] M. Baleeswaraiah, T.N. Narayanan, B. Kaushik, M.A. Pulickel, T. Saikat, 2D Mater 1 (1) (2014), 011008.
[49] Y. Zhang, J.R. Choi, S.-J. Park, Composites Part A 101 (2017) 227–236.
[50] Y. Zhang, K.Y. Rhee, S.-J. Park, Composites Part B 114 (2017) 111–120.
[51] H. Gu, J. Guo, X. Yan, H. Wei, X. Zhang, J. Liu, Y. Huang, S. Wei, Z. Guo, Polymer 55 (17) (2014) 4405–4419.
[52] K. Zhang, G.-H. Li, L.-M. Feng, N. Wang, J. Guo, K. Sun, K.-X. Yu, J.-B. Zeng, T. Li, Z. Guo, M. Wang, J. Mater. Chem. C 5 (36) (2017) 9359–9369.
[53] V. Lordi, P. Erhart, D. Åberg, Phys. Rev. B Condens. Matter 81 (23) (2010), 235204.
[54] A. Fert, Rev. Mod. Phys. 80 (4) (2008) 1517–1530.
[55] H. Gu, X. Zhang, H. Wei, Y. Huang, S. Wei, Z. Guo, Chem. Soc. Rev. 42 (13) (2013) 5907–5943.
[56] T.V. Laptyeva, J.D. Bodyfelt, D.O. Krimer, S. Ch, S. Flach, EPL (Europhys Lett) 91 (3) (2010), 30001.
[57] B.R. Matis, F.A. Bulat, A.L. Friedman, B.H. Houston, J.W. Baldwin, Phys. Rev. B Condens. Matter 85 (19) (2012), 195437.
[58] M. Liu, J. Zhang, C.-Z. Chang, Z. Zhang, X. Feng, K. Li, K. He, L-l Wang, X. Chen, X. Dai, Z. Fang, Q.-K. Xue, X. Ma, Y. Wang, Phys. Rev. Lett. 108 (3) (2012), 036805.
[59] M. Houshiar, F. Zebhi, Z.J. Razi, A. Alidoust, Z. Askari, J. Magn. Magn Mater. 371 (2014) 43–48.
[60] Y. He, S. Yang, H. Liu, Q. Shao, Q. Chen, C. Lu, Y. Jiang, C. Liu, Z. Guo, J. Colloid Interface Sci. 517 (2018) 40–51.
[61] H. Gu, C. Ma, J. Gu, J. Guo, X. Yan, J. Huang, Q. Zhang, Z. Guo, J. Mater. Chem. C 4 (25) (2016) 5890–5906.
[62] AF Jr., FCe Silva, Appl. Phys. Lett 96 (17) (2010), 172505.
[63] T.E. Quickel, V.H. Le, T. Brezesinski, S.H. Tolbert, Nano Lett. 10 (8) (2010) 2982–2988.
[64] N.R. Rao, A. Gabay, G. Hadjipanayis, J. Phys. D Appl. Phys. 46 (6) (2013), 062001.
[65] F.J. Pedrosa, J. Rial, K.M. Golasinski, M. Rodriguez-Osorio, G. Salas, D. Granados, J. Camarero, A. Bollero, RSC Adv. 6 (90) (2016) 87282–87287.